Star formation rate in spiral galaxies

Mattia Carraro, Daniele Moretto, Filippo Stellin, Gianluca Stellin

Liceo Scientifico "Galileo Galilei", Dolo (VE)

ABSTRACT

We have calculated the star formation rate, the number of solar masses annually formed, in 20 spiral galaxies. Moreover it has been possible to establish the number of ionizing photons and the theoretical number of 05 stars needed to produce these emissions. The twenty galaxies have been selected from the SDSS Data release 6 database.

I. INTRODUCTION

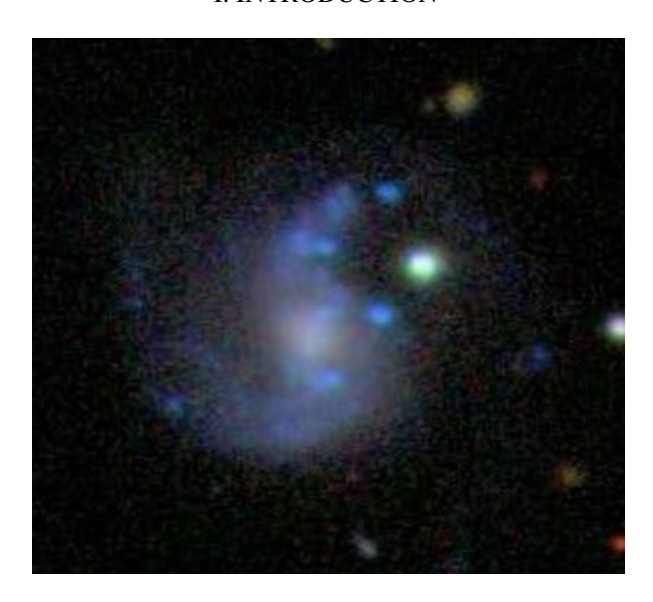
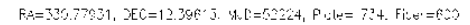


Figure 1: The object SDSS J143245.14+025454.0, it is an example of a barred spiral galaxy.

The computation of the star formation rate (SFR) was accomplished on twenty spiral galaxies, which were accurately selected from a database, according to specific criteria. The objects that were identified have redshifts that range from 0 to 0.035, clearly visible H α and H β emission lines, and a high brightness in the g band. In this way, only galaxies rich in young and hot stars were chosen, avoiding elliptical galaxies, which generally have old stars.

II. OBSERVATIONAL DATA

The spiral galaxies chosen for our project were already supplied with data regarding their astronomic coordinates (right ascension and declination), their redshift value z and the fiber magnitudes in filters u, g, r, i, z.



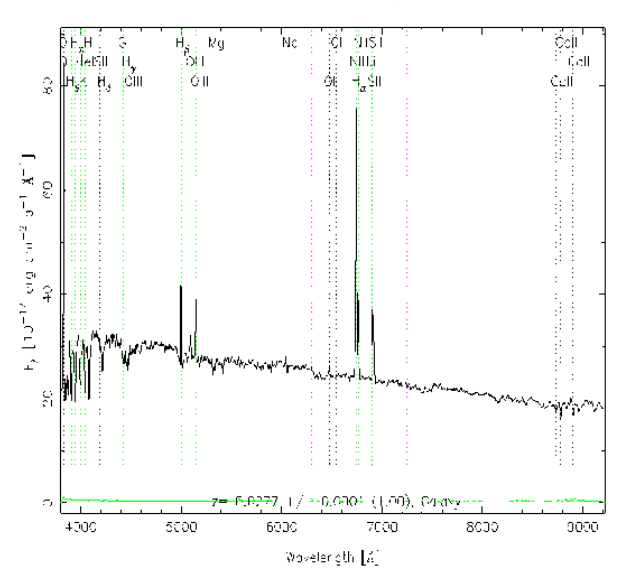


Figure 2: The spectrum of the object SDSS J220307.02+122346.0. An example of a spectrum that shows marked H α and H β emissions.

The fiber magnitudes refer to the flux contained within a circular aperture of 3" in diameter centered on the objects.

The data collected from the studied galaxies are reported in table 1 at the end of this report.

III. WORK DESCRIPTION

To begin, we downloaded from the SDSS Data Release 6 a list of 2000 galaxies with z value that ranges from 0 to 0.03. According to the color-color diagram *u-g* vs. *g-r* we selected 20 galaxies with blue color indices.

Then, we analyzed the spectrum of each galaxy with IRAF, in order to obtain the wavelengths of the emission peaks corresponding to $H\alpha$, $H\beta$ and [OIII] lines. We compared these wavelengths with rest frame values (that are respectively 6563Å, 4861Å and 5007Å) to measure again their redshifts.

$$z = \frac{\frac{\lambda_{H\alpha}^{'} - \lambda_{H\alpha}}{\lambda_{H\alpha}} + \frac{\lambda_{H\beta}^{'} - \lambda_{H\beta}}{\lambda_{H\beta}} + \frac{\lambda_{OIII}^{'} - \lambda_{OIII}}{\lambda_{OIII}}}{3}$$

The z values were used to calculate the galaxies' distance (expressed in Mpc), applying Hubble's law:

$$d = \frac{c \cdot z}{H_{\circ}}$$

where c is 299700 km·s⁻¹ and the Hubble's constant H_o is equal to 72 km·Mpc⁻¹·s⁻¹.

With the same software, we measured the fluxes of the emission lines H α and H β (expressed in 10^{-17} erg \cdot s $^{-1}$ · cm $^{-2}$), that were expected to be significantly different in comparison to the real fluxes emitted by the galaxies. This difference is caused by the *extinction* phenomenon, due to cosmic dust absorbing part of the emitted radiation, in particular at short wavelengths: consequently, the flux appears very reduced in the blue and violet bands.

This effect occurs mainly inside each galaxy, but it is also influenced by the galaxy position relatively to the Milky Way, since the light passes through different dust layers of the Galaxy.

The spectra of our galaxies were corrected for the Milky Way extinction using the task *deredden* and the A(V) values given by NED (NASA Extragalactic Database).

To correct the measured emission line fluxes, we applied the following empirical law, given by Cardelli, Clayton e Mathis [CCM 1989]:

$$\frac{A(\lambda)}{A(V)} = a(y) + \frac{b(y)}{R(V)}$$

At first we determined the value of the *y parameter* related to $\lambda_{H\alpha}$ (6563Å) and $\lambda_{H\beta}$ (4861Å):

$$y = \frac{10^4}{\lambda} - 1.82$$

$$y_{H\alpha} = -0.2963$$
 and $y_{H\beta} = 0.2372$

In this way, we found the values of the parameters a e b characteristic of each wavelength, applying the following polynomial equations:

$$\begin{array}{l} a(y) = 1 \ + \ 0.17699y \ - \ 0.50447y^2 \ - \ 0.02427y^3 \ + \\ 0.72085y^4 + 0.01979y^5 - 0.77530y^6 + 0.32999y^7 \end{array}$$

$$\begin{array}{l} b(y) = 1.41338y + 2.28305y^2 + 1.07233y^3 - 5.38434y^4 \\ -0.62251y^5 + 5.30260y^6 - 2.09002y^7 \end{array}$$

$$a_{H\alpha} = 0.9088$$
; $b_{H\alpha} = -0.2823$

$$a_{H\beta} = 1.0154$$
; $b_{H\beta} = 0.4613$

The selective ratio R(V), on the other hand, depends on the size of the dust grains, which absorb photons, and can have values between 3 and 7: in general, the value 3.1 is adopted.

We calculated the extinctions $A(H\alpha)$ and $A(H\beta)$, replacing the parameters a, b and R(V) in the empirical law mentioned above:

$$A(H\alpha) = 0.8177 \cdot A(V)$$
 [1]
 $A(H\beta) = 1.1642 \cdot A(V)$ [2]

In the following graph the absorption as a function of wavelengths is reported.

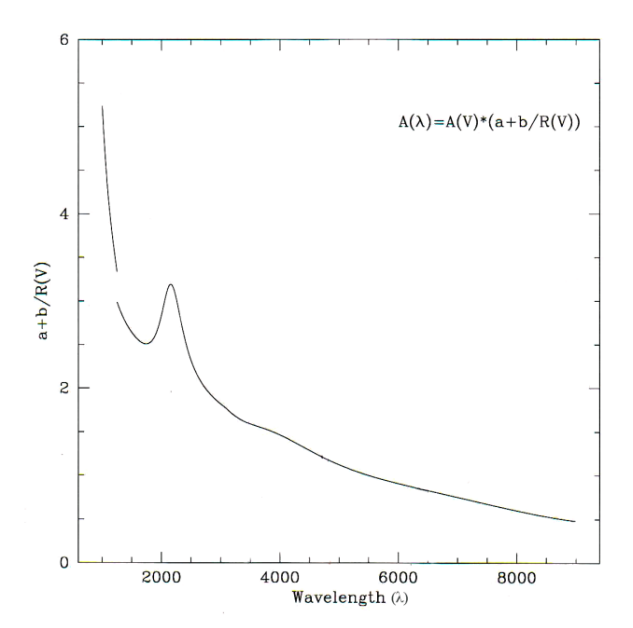


Figure 3: CCM (1989) reddening function.

The wavelength is on the x-axis, while on the y-axis there is the ratio between the absorption in a specific λ and the one corresponding to the photometric V band (centered at 5500Å). We can notice that this ratio increases rapidly at short wavelengths, and reaches values near to zero in the infrared.

Since the value of the absorption at a certain wavelength coincides with the difference between the observed and the real magnitudes at that wavelength, from the Pogson law we derive:

$$A(\lambda) = m_0 - m = -2.5 \log_{10} \left(\frac{F_0}{I} \right)$$

where m_0 is the observed magnitude, while m is the magnitude that the galaxy should have if the radiation were not absorbed.

Consequently, F_0 is the observed flux, and I is the intrinsic flux: in our case F_0 was replaced with the measured fluxes $F_{H\alpha}$ e $F_{H\beta}$:

$$A(H\alpha) = -2.5 \log_{10} \left(\frac{F_{H\alpha}}{I_{H\alpha}} \right)$$

$$A(H\beta) = -2.5 \log_{10} \left(\frac{F_{H\beta}}{I_{H\beta}} \right)$$

Afterwards, we deduced the following equations by exploiting the logarithm properties:

$$\frac{F_{H\alpha}}{I_{H\alpha}} = 10^{-0.4 \cdot A(H\alpha)}$$

$$\frac{F_{H\beta}}{I_{H\beta}} = 10^{-0.4 \cdot A(H\beta)}$$

Then, we obtained the equation of the intrinsic flux ratio:

$$\frac{I_{H\alpha}}{I_{H\beta}} = \frac{F_{H\alpha}}{F_{H\beta}} \cdot 10^{0.4 \cdot A(H\alpha - H\beta)}$$

By replacing $A(H\alpha)$ and $A(H\beta)$ with the equation previously mentioned and given that the intrinsic ratio is 2.86 (Balmer Decrement), we obtained:

$$\frac{I_{H\alpha}}{I_{H\beta}} = 2.86 = \frac{F_{H\alpha}}{F_{H\beta}} \cdot 10^{-0.1386A(V)}$$

from which we have:

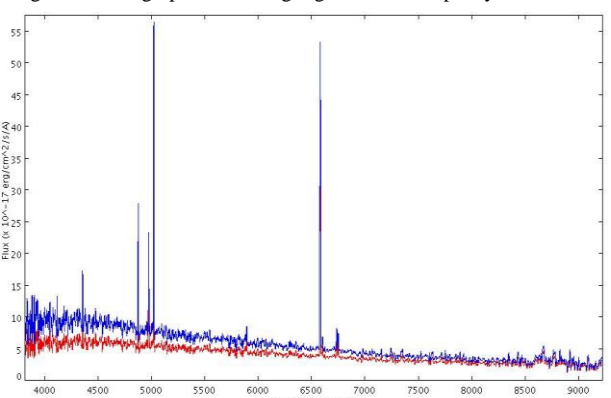
$$A(V) = \frac{\log(2.86) - \log\left(\frac{F_{H\alpha}}{F_{H\beta}}\right)}{-0.1386}$$

At last, we could calculate the intrinsic fluxes $I_{H\alpha}$ and $I_{H\beta}$, starting from the previous equations:

$$I_{H\alpha} = F_{H\alpha} \cdot 10^{0.3271 A(V)}$$

$$I_{H\beta} = F_{H\beta} \cdot 10^{0.4657 A(V)}$$

Figure 4: The graph above highlights the discrepancy between the



real fluxes (in blue) and the observed ones (in red): the high-frequency radiation absorbed by the interstellar medium is emitted at longer wavelengths, in the nearby infrared. The spectrum belongs to the object SDSS J002908.36+155356.8, an Sb galaxy.

Then, we transformed fluxes into luminosities using the distances calculated earlier:

$$L = 4\pi d^2 \cdot I$$

From the fiber magnitudes in u and g filters, we first calculated the apparent magnitude B that corresponds to an aperture of 3 arcseconds on the galaxy centers:

$$B = g - 0.17 \cdot (u - g) + 0.11$$

And, after that, the absolute B magnitude:

$$M_B = m_B + 5 - 5\log(d)$$

where the distance d is expressed in parsec.

Comparing M_B with the solar absolute magnitude $M_{B(o)}$ =+5.48 and his luminosity L_o = 3.9E33 erg/s, we calculated the B luminosity for each galaxy using the formula:

$$L_B = L_{Sun} \cdot 10^{\frac{M_B - M_{B,Sun}}{-2.5}}$$

With the software TopCat, we reported each galaxy in a graph of luminosity of $H\alpha$ emission line (x-axis) versus the B luminosity (y-axis). We used a logarithmic scale and calculated with TopCat the best linear regression function. The data follow a linear function, $log(L_B) = m \cdot log(L_{H\alpha}) + q,$ with slope m=0.997 and intercept q=2.17.

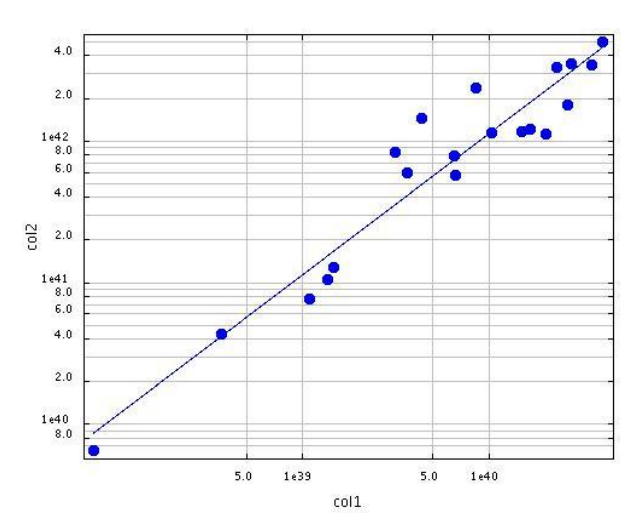


Figure 5: Ha luminosity (x-axis) versus B luminosity (y-axis).

Why a similar relation exists? In order to observe the ionized gas, it is necessary the presence of hot stars (O, B). If there are hot stars, they are so bright that they give substantial contribution to the galaxy radiation. Taking into account the black body function, we know that hot stars contribute more at shorter wavelengths, therefore in the photometric bands U and/or B. In conclusion, even if B and H α luminosities were derived independently, they share the same origin: the presence of hot and bright stars.

As we have previously underlined, the data through which we obtained L_B and $L_{H\alpha}$ are referred only to the central part of the galaxies. In order to give a rough estimate of the $H\alpha$ luminosity of the entire galaxy, we extracted the total magnitudes in the u and g filters from the SDSS Database, and we repeated the same calculations, obtaining the total B luminosity for each galaxy.

Under the hypotheses that the $L_{H\alpha}\text{-}L_B$ relation found earlier can be applied also to the entire galaxies and that ionized gas is homogeneously distributed within each galaxy, we calculated the total $L_{H\alpha}$ with the equation:

$$L_{H\alpha-TOT} = 10^{\frac{\log L_{B-TOT}-2.17}{0.997}}$$

Obtained so forth the energy emitted in the H α line by each galaxy, we found the respective number of *ionizing photons* giving origin to that energy emission:

$$Q_{ion} = 7.3 \cdot 10^{11} \cdot L_{H\alpha-TOT}$$

And the star formation rate, expressed in solar masses per year:

$$SFR = 7.9 \cdot 10^{-42} \cdot L_{H\alpha-TOT}$$

IV. RESULTS

The intensity of the $H\alpha$ emission line increases proportionally to the number of hot stars contained in a galaxy, because they are able to produce a significant amount of ionizing photons (having energy higher than 13.6 eV).

If we consider that an O5 star emits about $10^{49.67}$ ionizing photons/sec, we can give an estimate of the expected number of O5 stars in each galaxy:

$$N(O5) = \frac{Q_{ion}}{10^{49.67}}$$

Even if the $H\alpha$ emission is clearly not caused exclusively by O5 stars, which are also very rare, this number can be useful to compare the possible number of young and hot stars in each galaxy.

Therefore, among our galaxies, there are some of them that reach only 2400 O5 stars (like object 5 in the table below), while some other galaxies contain more than 500000 stars, like object 12. This happens because object 5 presents the lowest SFR of the twenty galaxies (only 0.29 $\rm M_{\odot}/\rm yr)$, while object 12 possesses the highest one: it forms about 70 new solar mass stars each year.

High SFR values are tightly referred to galaxies with young star populations, in which the gas reemits the star radiation below Lyman's limit (912Å), in the UV region.

Therefore, only in galaxies containing stars with mass $20M_{\odot}$ and a lifetime less than 20 million years it is possible to measure relevant H α and H β fluxes, and also fluxes in P α , P β , Br α and Br γ lines.

Furthermore, the SFR depends also on the gas density and on the galaxy morphology (see Hubble's classification), and shows a remarkable range from zero in the gas-poor elliptical and S0, to $20~M_{\odot}/\text{yr}$ in gas-rich spirals. Much larger global SFRs, up to $100~M_{\odot}/\text{yr}$, can be found in optically selected starburst galaxies, and SFRs as high as $1000~M_{\odot}/\text{yr}$ may be reached in the most luminous IR starburst ones, as the following table shows.

Type	SFR (M∘•year ⁻¹)		
S0, elliptical, dwarf	→0		
spiral	20<>100		
starbursts	100<>1000		
IR starbursts	>>1000		

Considering all these factors, we may assert that galaxies similar to object 5, with SFR equal to 0.29 M_{\odot}/yr are dwarf spirals, while others like object 12, with values as high as 70 M_{\odot}/yr can be classified as large spirals (normal or barred).

V. BIBLIOGRAPHY

R. C. Kennicutt jr., *Star Formation in Galaxies along the Hubble Sequence*, Annu. Rev. Astron. Astrophys. 1998. 36:189–231, (1998);

Report on a stage of Asiago, M. Lazzari, M. Rocchetto, I. Vidal, *Misura della Star Formation Rate nelle galassie NGC 1569, NGC 2798 e NGC 3227,* 2006/2007 Edition;

Report on a stage of Asiago, F. Barato, E. Battistich, G. Martignon, *Determinazione del tipo spettrale e stima dell'estinzione in stelle con righe di emissione*, 2002/2003 Edition;

Cardelli J.A., Clayton G.C., Mathis J.S., *The Relationship between infrared, optical and ultraviolet extinction*, Ap.J. 345:245-256 (1989);

VI. DATA TABLES

	fiberMag		TotMag		Distance (Mpc)
ObjectID	u	g	u	g	
SDSS J141318.93+013951.8	20.5821	19.2101	18.00	16.75	108.960
SDSS J124745.92+030851.5	20.1333	19.1071	18.94	18.01	87.949
SDSS J093437.00+000245.8	19.6967	18.6693	17.66	16.73	69.165
SDSS J092223.10+504628.9	20.1346	19.0591	17.98	16.99	112.996
SDSS J002908.36+155356.8	20.8136	20.0397	17.67	16.52	11.681
SDSS J024120.21-071705.9	20.4400	19.5706	17.97	17.11	24.348
SDSS J130049.13-012136.4	20.5879	19.6888	18.51	17.58	95.760
SDSS J115314.09-032432.2	18.4131	17.8685	17.00	16.27	18.507
SDSS J121214.73+000420.2	18.3725	17.4426	16.74	15.86	33.421
SDSS J151047.23-002053.9	20.4019	19.4784	17.24	16.17	31.173
SDSS J220307.02+122346.0	19.3559	18.1886	17.71	16.66	116.303
SDSS J141523.71+042430.6	19.1761	18.0893	15.72	14.83	81.057
SDSS J130158.45-034046.8	20.0605	18.8825	17.62	16.59	114.431
SDSS J143245.14+025454.0	19.3130	18.3930	15.79	14.91	22.303
SDSS J173206.08+583713.9	19.0540	18.1154	17.89	16.78	111.734
SDSS J215953.35+112045.1	20.4541	19.3163	18.99	17.87	115.041
SDSS J004118.34-094620.6	19.1990	18.0987	18.20	17.12	116.264
SDSS J135541.65+025215.9	18.2376	17.5065	16.91	15.97	100.053
SDSS J225520.60+130507.3	19.7685	18.8381	18.97	18.09	91.964
SDSS J153413.35+571707.0	18.0433	17.5226	16.55	15.86	47.636

ObjectID	$SFR (M_{\Theta}/yr)$	Ionizing photons	No O5 contained	B total Luminosity	Hα total Luminosity
SDSS J141318.93+013951.8	20.375	7.828E+54	167365	1.068E+43	1.072E+43
SDSS J124745.92+030851.5	4.373	1.680E+54	35921	2.292E+42	2.302E+42
SDSS J093437.00+000245.8	8.792	3.378E+54	72220	4.609E+43	4.627E+42
SDSS J092223.10+504628.9	18.296	7.030E+54	150292	9.591E+42	9.630E+42
SDSS J002908.36+155356.8	0.294	1.130E+53	2415	1.541E+41	1.547E+41
SDSS J024120.21-071705.9	0.776	2.982E+53	6376	4.069E+41	4.085E+41
SDSS J130049.13-012136.4	7.703	2.960E+54	63278	4.038E+42	4.054E+42
SDSS J115314.09-032432.2	0.992	3.812E+53	8150	5.201E+41	5.222E+41
SDSS J121214.73+000420.2	4.611	1.771E+54	37873	2.417E+42	2.427E+42
SDSS J151047.23-002053.9	2.927	1.124E+54	24040	1.534E+42	1.540E+42
SDSS J220307.02+122346.0	26.022	9.998E+54	213753	1.364E+43	1.370E+43
SDSS J141523.71+042430.6	69.923	2.687E+55	574367	3.665E+43	3.680E+43
SDSS J130158.45-034046.8	26.953	1.036E+55	221398	1.413E+43	1.419E+43
SDSS J143245.14+025454.0	4.925	1.892E+54	40458	2.582E+42	2.592E+42
SDSS J173206.08+583713.9	25.152	9.664E+54	206606	1.318E+43	1.323E+43
SDSS J215953.35+112045.1	8.262	3.174E+54	67869	4.331E+42	4.349E+42
SDSS J004118.34-094620.6	16.944	6.510E+54	139181	8.882E+42	8.918E+42
SDSS J135541.65+025215.9	36.991	1.421E+55	303853	1.939E+43	1.947E+43
SDSS J225520.60+130507.3	4.477	1.720E+54	36773	2.347E+42	2.356E+42
SDSS J153413.35+571707.0	9.649	3.707E+54	79263	5.058E+42	5.079E+42